Noncatalytic and Finite Catalytic Heating Models for Atmospheric Re-entry Codes

Ysolde Prevereaud, Jean-Luc Vérant, Julien Annaloro

Noncatalytic and Finite Catalytic Heating Models for Atmospheric Re-entry Codes

Ysolde Prévereaud[(1)], Jean-Luc Vérant[(1)], and Julien Annaloro[(2)]

[(1)] ONERA – The French Aerospace Lab. – 2 avenue Edouard Belin, 31055 Toulouse – France, ysolde.prevereaud@onera.fr, jean-luc.verant@onera.fr
[(2)] CNES – 18 avenue Edouard Belin, 31400 Toulouse – France, Julien.Annaloro@cnes.fr

ABSTRACT

The total wall heat flux is one of the key quantities in the evaluation of the ground risk associated to debris atmospheric entry. The computed heat flux assuming catalytic wall or thermochemical equilibrium gas can be twice as large as the non-catalytic wall heat flux, leading to an underestimation of the ground risk. However, most of the models proposed in open literature allow computing stagnation point heat flux for thermochemical equilibrium air gas or chemical nonequilibrium air gas with catalytic walls only, or requires many local quantities that are not yet accessible for engineering atmospheric codes. For these reasons, ONERA developed and successfully validated new analytical models to compute the total heat flux received by the wall assuming any inflow gas state as well as finite-catalytic and non-catalytic wall material properties. These new models have been developed from a large in-house CFD database built-up with the ONERA Navier-Stokes code for various flow conditions (altitude from 70 to 20 km, velocity from 8 to 1 km/s) including different thermochemical air flow assumptions in the shock layer (perfect gas, thermochemical equilibrium and nonequilibrium real gas), effects of the nose radius (from 0.01 m to 1 m) and wall temperature (from 300 K to 2000 K). The present paper proposes an overview of the current research with a focus on the new models developed and their application relevant to on the aerothermodynamic study of the atmospheric entry of a launcher tank. A specific attention is given to the influence of the wall catalycity on the thermal degradation of such debris.

1 INTRODUCTION

Since 1957 and the orbital performance of the soviet satellite Spoutnik-1, the human activity in space has generated a great number of space debris. Currently, about 15,000 debris larger than 1 cm lie in Earth orbit [1]. A large part of the orbital debris ranging from ten microns to several meters executes an atmospheric entry due to atmospheric drag in LEO and lunisolar perturbations in HEO (acting generally with atmospheric drag). Between 1957 and 2017 about 75% of all the larger objects ever launched have performed a reentry [2]. Only a small percentage was subjected to an intentional deorbiting or reached the ground under control. Currently, only few very large objects cross Earth's atmosphere per year. Objects of moderate size, 1 m or above, re-enter around once a week, while an average of two small tracked debris objects re-enters per day. Between 10 and 40 % of the debris mass are estimated to have reached Earth surface [3], representing a potential threat to ground safety. An estimate of the total causality area becomes a major issue for all space actors and especially for CNES which is in charge of ensuring the right application of the French Space Operation Law (LOS) that will enter into force by 2021 for both French satellites and launchers operators as well as launching operations from French Guyana spaceport.

These space actors have developed tools dedicated to the prediction of the ground risk generated by space debris atmospheric re-entry. Indeed, high fidelity physical models as those of CFD tools (Fluid mechanics and energetics equations) cannot characterize a whole trajectory described by the hundreds of points needed by a Monte Carlo procedure aiming at assessing uncertainties in relation to the ground risk estimate. Only a strategy based on relevant and reliable reduced models is acceptable for debris risk analysis in terms of computing time and computing capability. These engineering tools can be separated into two categories: Object-Oriented Codes and Spacecraft-Oriented Codes. Object-Oriented Codes consider individual satellite parts only. Therefore, this kind of code assumes that at a given altitude the satellite is decomposed into its elementary items. In other words, Object-Oriented Codes reduce the complex analysis of the atmospheric re-entry of a spacecraft to the simple analysis of its most critical parts, which must be previously defined by the user. The fragmentation altitude discussed in [14] is usually fixed to 92 km beginning with the solar panel fragmentation and between 75 and 85 km for total fragmentation of the debris. Major Object-Oriented Codes described into open literature are DAS/ORSAT (NASA) [4], DRAMA/SESAM (ESA) [6] and DEBRISK (CNES) [7]. DEBRISK will be used as a certification tool in the frame of the application of the LOS.

On the other side, Spacecraft-Oriented Codes simulate the whole satellite taking into consideration the most realistic design. Analytical models are also used to predict wall pressure and heat flux distributions on the whole 3D surface of the debris, from which are inferred aerodynamic forces and moments, and local mass ablation at each timestep of the atmospheric trajectory. The fragmentation model generates the fragments facing the harsh environment encountered during such re-entry. After each break-up process, each fragment is analyzed individually with regards to ablation mechanism and its modelling. SCARAB (HTG) [11], PAMPERO (CNES) [12] and ARES (ONERA) [13] are some of the major or published European Spacecraft-Oriented Codes.

The wall heat flux is one of the key quantities whose ground risk estimate depends on. Its evaluation, which must be as close as possible to the reality, depends on the wall catalysis, the thermochemical state of the flow around the object and the type of material at the wall. Silica and ceramics tend to be non-catalytic whereas metals and alloys are rather highly catalytic; catalycity also increasing with temperature. Most of the models proposed in open literature, such as Detra [10] [16], Scott [8], Sutton-Graves [27], Vérant-Sagnier's models [9], allow computing stagnation point heat flux for thermochemical equilibrium gas or chemical nonequilibrium gas with full catalytic walls only. However, it must be noticed that computed heat flux assuming catalytic wall or thermochemical equilibrium gas can be twice as large as the non-catalytic wall heat flux, inducing an underestimation of the ground risk. Even though Fay-Riddell [21] proposed a formulation to compute stagnation point heat flux for frozen gas with non-catalytic wall, this model requires many local flow quantities that are not accessible for engineering atmospheric codes.

This paper presents new models developed by ONERA and successfully validated to compute the total heat flux balance at wall for any inflow gas state assuming finite and non-catalytic wall properties. A study of the influence of the wall catalycity on the thermal degradation of space debris is proposed.

2 WALL CATALYCITY

At microscopic level, heterogeneous catalysis, between a solid catalyst and gaseous reactants, takes place in three steps: 1) **Adsorption**: Particles diffusing to the wall can either undergo specular reflection or be adsorbed by the surface. Only the chemisorption, which is the creation of chemical bonds between particles of the surface and adsorbed particles, can lead to catalysis process. This first step depends on the particles striking the wall surface and the surface itself. For example, metallic surfaces can easily adsorb oxygen atoms. In general, heterogeneous catalysis is favored when the energy barrier associated to adsorption process is weaker than the one of the chemical reactions in the gas. 2) **Recombination**: Adsorbed atoms can move over the surface and recombine with another adsorbed particle (Langmuir-Hinshelwood recombination). Recombination can also occur when a gas atom strikes an adsorbed particle by breaking bonds between the adsorbed particle and the surface (Eley-Rideal recombination). 3) After recombination process, particles leave the surface and return into the flow: **Desorption**.

The problem is complex as various species can be simultaneously adsorbed and lead to different catalysis reactions at the material surface. Moreover, heterogeneous catalysis depends mainly on the surface capacity to adsorb gaseous species and thus greatly depends on the material.

The catalytic production/destruction rate $q_{cat,I}$ is expressed as:

$$q_{cat,I} = k_{wI}\, \rho_I^{m_I} \tag{1}$$

where k_{wI} is the reaction rate constant, whose unit depends on the chemical order of the reaction m_I, and ρ_I is the partial density of reactants. Mass conservation at the surface imposes that the catalytic production/destruction rate is equal to the species diffusion flux at the wall. The challenge is to model the reaction rate constant for the reactions occurring at the surface. Different models with different approximation levels are proposed in the literature.

In 1958, Goulard [17] introduced simple catalytic model describing the reaction rate constant k_{wI} of the species I with the recombination coefficient γ_I:

$$k_{wI} = \gamma_I \sqrt{\frac{k_B T_w}{2\pi m_I}} \tag{2}$$

where k_B is the Boltzmann constant (in J/K) and T_w is the wall temperature (in K). The recombination coefficient is the ratio between the mass flux of atoms recombining at the surface and the mass flux of atoms impinging the surface.

Finite Rate Chemistry (FRC) models, widespread in open literature, associate a reaction rate constant k_w to each elementary step (adsorption, Langmuir-Hinshelwood recombination, Eley-Rideal recombination, desorption) to describe heterogeneous catalysis. However, this kind of models will be not described in this paper.

When the reaction rate constant approaches infinity, species impacting the wall react very quickly. The flow near the wall approaches chemical equilibrium: the wall is catalytic (Fig. 1). When the reaction rate constant tends toward zero ($k_w = \gamma = 0$), the wall is considered non-catalytic, meaning that no atom impinging the wall recombine. Finally, the wall can be partially catalytic; some atoms recombine while others do not.

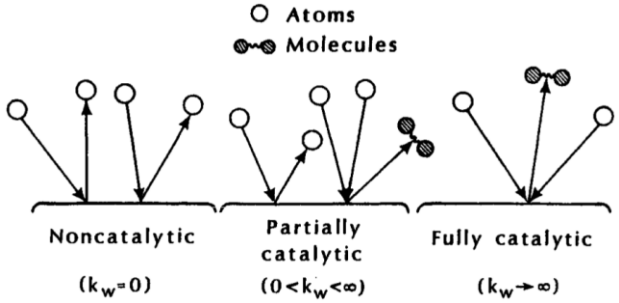

Fig. 1. Effect of the wall catalycity on atoms recombination [16].

It is commonly assumed that all the energy due to recombination is transmitted to the wall, even if measurements [18], [19] have shown that it is not the case, and that molecules could leave the surface in an excited state. Measurements in air plasma jets have shown that wall catalycity varies with time; in other words, a material rather catalytic becomes more and more catalytic. Two phenomena may explain this evolution: the adsorption-desorption process modifies the surface, increasing the surface porosity and thus the number of available sites. On the other hand, these changes at the wall surface could modify the surface emissivity. This is in accordance with the rise of the Space Shuttle wall heat flux observed between the flight STS-2 to STS-5 for the same trajectories [20].

3 NUMERICAL SIMULATION OF THE WALL CATALYCITY

3.1 PRESENTATION OF THE NUMERICAL SIMULATION

ONERA developed an important in-house CFD database, including around 200 Navier-Stokes simulations, for various upstream flow conditions (altitude from 70 to 20 km, velocity from 8 to 1 km/s) leading to different thermochemical flow conditions in the shock layer (perfect gas, frozen gas, thermochemical equilibrium and chemical nonequilibrium gas), effects of the nose radius (from 0.01 m to 1 m), wall temperature (from 300 K to 2500 K), and recombination coefficient (from 0 to 1; 0: non-catalytic, 1: catalytic).

Numerical simulations have been performed with the ONERA code CELHyO. According to the number of simulations to realize, CELHyO 2D/3D equivalent approach has been used. This approach is based on a mono-dimensional reduction of the Navier-Stokes equations. Stagnation values are obtained with a precision always inferior to 1% compared to 2D and 3D simulations performed respectively for a sphere and the X38 vehicle with the ESA CFD code LORE. Navier-Stokes equations are discretized by a second order finite volume method in space and a HUS flux scheme associated to a Minmod limiter. The flow is assumed laminar and in chemical nonequilibrium based on the Park's kinetics (with 5 species and 17 reactions) to assume real gas effect occurring at high Mach numbers. However, the gas conditions depend on the flight point, the form and the attitude of the object. According to these parameters, the flow computed by CELHyO can be locally a perfect gas or a real gas at thermochemical equilibrium or chemical non-equilibrium state. Therefore, the gas condition is not fixed by the user but by the local flow conditions.

For a non-catalytic wall, the mass fraction gradient at the wall is set to zero. For a catalytic wall, thermochemical equilibrium is assumed at the wall to compute both wall pressure and temperature conditions. For a finite catalytic wall, the recombination coefficient has been imposed, assuming that $\gamma_O = \gamma_N$.

3.2 ANALYSIS OF THE NUMERICAL RESULTS

The influence of various parameters, such as the nose radius (Fig. 2), the wall temperature (Fig. 3), the flight point (Fig. 2 to Fig. 4), and the recombination coefficient γ (Fig. 4), on the stagnation point heat flux and wall enthalpy is

analysed in this section. As a general remark, the CFD results underline the interactions between these parameters and their coupled influence on the stagnation point heat flux and wall enthalpy.

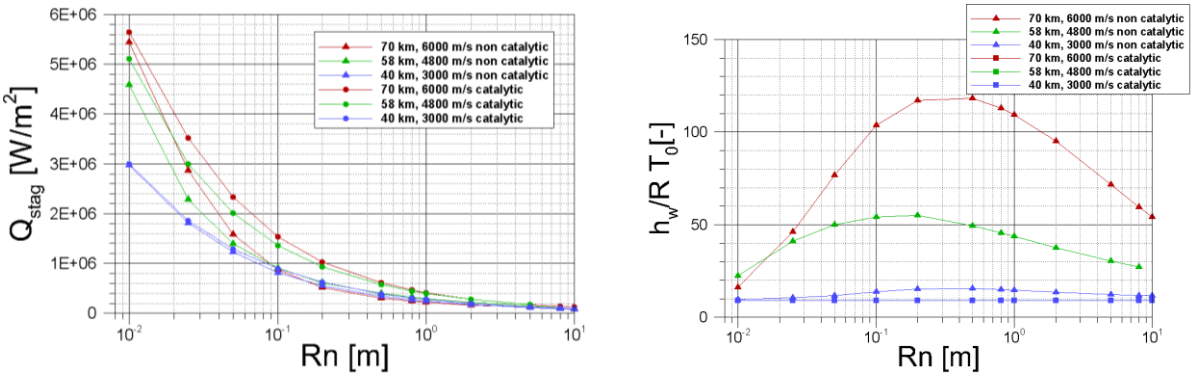

(a) (b)

Fig. 2. Influence of the nose radius on the wall stagnation point heat flux (a) and wall enthalpy (b) for various flight points and $T_w = 700\ K$.

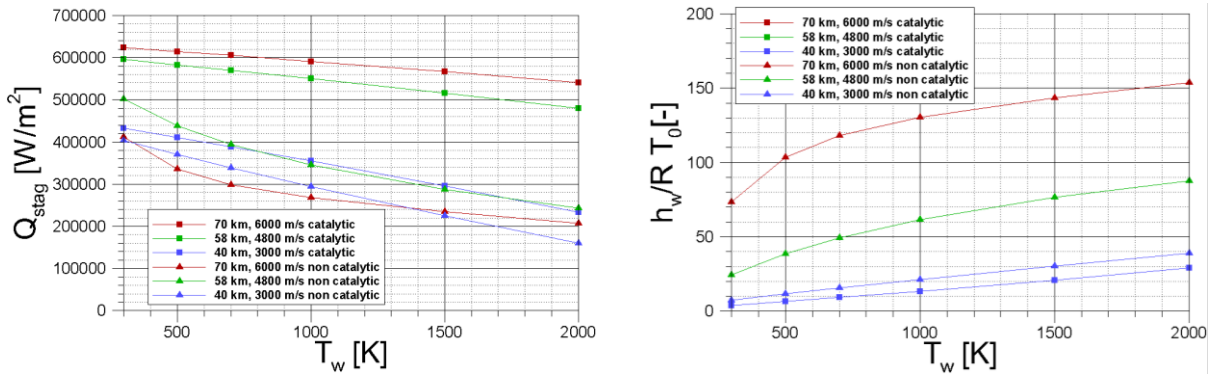

(a) (b)

Fig. 3. Influence of the wall temperature on the stagnation point heat flux (a) and wall enthalpy (b) for various flight points and $Rn = 0.5\ m$.

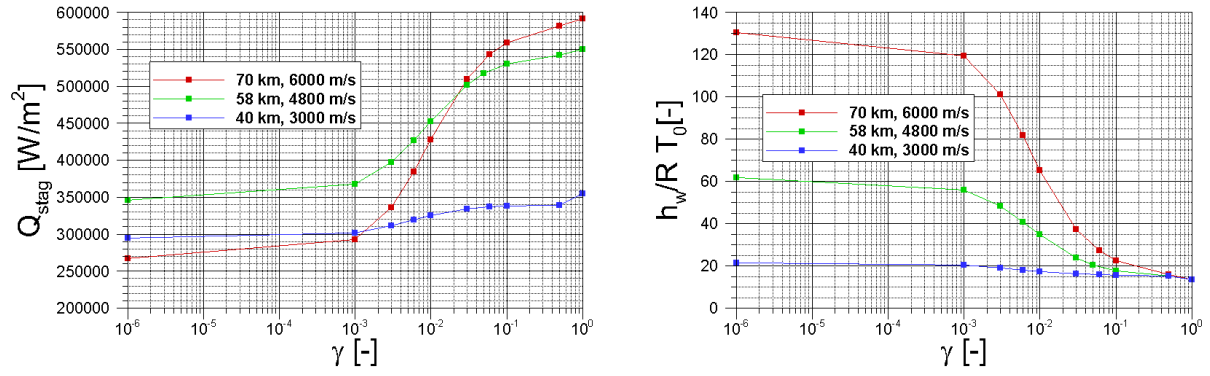

(a) (b)

Fig. 4. Influence of the value of the recombination coefficient γ on the stagnation point heat flux (a) and wall enthalpy (b) for various flight points, $Rn = 0.5\ m$ and $T_w = 1000\ K$.

As highlighted by Zoby *et al.* [5] and illustrated in Fig. 2.a, the wall heat flux decreases and tends towards the thermochemical equilibrium one when the nose radius rises, regardless of the flight point and the wall catalysis. On

the other hand, for very small and very high nose radii, specific enthalpy tends to be independent of Rn and reaches a minimum value which is the one obtains for a catalytic wall. When the nose radius increases, the shock standoff distance logically increases. By this way, the ratio between the characteristic time associated to the particles motion in the shock layer and the characteristic time of the chemical reactions is modified, inducing a local modification of the flow conditions. Indeed, the rise of the shock-boundary layer distance favours the atoms recombination and a very limited number of atoms reaches the wall. Thus, the stagnation heat flux level tends towards the one obtained when the flow is in thermochemical equilibrium. As shown in Fig. 2.a, the stagnation wall heat flux becomes independent of the nose radius for $Rn \geq 0.1\ m$ for a non-catalytic wall.

As illustrated by Fig. 3 and as expected, the stagnation point heat flux decreases while enthalpy increases with the wall temperature rise, regardless of the wall catalysis.

The stagnation point heat flux (Fig. 4.a) and enthalpy (Fig. 4.b) both follow a S curve according to the recombination coefficient γ as previously underlined by Fay-Riddell [21].

As exhibited in Fig. 2 to Fig. 4, the wall heat flux varies with the flight point (altitude, velocity) regardless the wall catalysis. Meanwhile, the enthalpy becomes independent of both the flight point and the nose radius for a catalytic wall. This property is no more verified for a non-catalytic wall.

4 THE CHALLENGES

In this section analytical models proposed in open literature or in the ONERA Spacecraft-Oriented code ARES are discussed and evaluated by comparison with results from CFD simulations. The objective is to evaluate the performance of the analytical models and to propose some improvements accordingly to solutions from CFD databases. In the sake of simplicity, following analysis will be realized for Fay-Riddell [21] and Sutton-Graves [27] formulations only; Verant-Sagnier equation [9] being similar to the Sutton-Graves one. Furthermore, the stagnation point heat flux equations proposed by Detra [10] and Scott [8] do not depend on the wall enthalpy, a behavior which disagrees with the results of the CFD simulations.

Fay and Riddell [21] propose the following formulation to compute stagnation point heat flux Φ_w for catalytic (Eq. 3) and non-catalytic (Eq. 4) wall and a frozen flow condition (weak recombination rate).

$$\frac{\Phi_w}{h_w - h_{ie}} = 0.76 \left(\wp \frac{\rho_e \mu_e}{\rho_w \mu_w}\right)^{0.4} \frac{1}{\wp} \sqrt{\rho_w \mu_w \left(\frac{dU_e}{dx}\right)_0} \left(1 + [\mathcal{L}^{0.63} - 1] \frac{h_{De}}{h_{ie}}\right) \tag{3}$$

$$\frac{\Phi_w}{h_w - h_{ie}} = 0.76 \left(\wp \frac{\rho_e \mu_e}{\rho_w \mu_w}\right)^{0.4} \frac{1}{\wp} \sqrt{\rho_w \mu_w \left(\frac{dU_e}{dx}\right)_0} \left(1 - \frac{h_{De}}{h_{ie}}\right) \tag{4}$$

Here, the subscript 0 refers to the stagnation point value, w to the wall values and e to values outside the boundary layer. h_D is the dissociation enthalpy per mass unit, i.e. formation enthalpy of atoms weighted by their corresponding mass fraction. h_i is the total enthalpy. $\wp$ is the Prandtl number and $\mathcal{L}$ the Lewis number. ρ, μ and U are respectively the flow density, viscosity and velocity. According to authors, these equations are valid for altitudes between 36 km and 7.5 km, flow velocity between 7 km/s and 1.8 km/s and wall temperature between 300 k and 3000 K.

Sutton and Graves [27] propose a general formulation (Eq. 5) for the stagnation point heat flux for a flow in thermochemical equilibrium, and valid for the Earth, Mars and Jupiter atmospheres.

$$\Phi_{\mathrm{w}} = K \sqrt{\frac{p_e}{R_N}} (h_{ie} - h_w) \tag{5}$$

Here K is a heat transfer coefficient, p_e is the stagnation point pressure outside the boundary layer, and R_N is the nose radius.

Lots of variables are not accessible to engineering software and need to be approximated by simplified models, especially for the Fay-Riddell equations that include local variables.

The total enthalpy outside the boundary layer is equal to the freestream enthalpy since its value is constant across a normal shock wave for an adiabatic flow: $h_{ie} = H_\infty = Cp\ T_\infty + V_\infty^2/2$. Pressure p_e, density ρ_e and dynamic viscosity

μ_e outside the boundary layer are given by the stagnation point properties computed by Rankine-Hugoniot equations and isentropic compression assuming thermochemical equilibrium flow conditions in the shock layer. This assumption leads to uncertainties up to 15% on ρ_e, 10% on μ_e and 10% on p_e compared to CFD CELHyO results.

One of the simplest models to compute the tangential velocity gradient at stagnation point $\left(\frac{dU_e}{dx}\right)$ is introduced by Lees [22]: it is based on the 1D formulation of the moment equation for a streamline near the stagnation point and used a Newtonian pressure distribution on a sphere: $\left(\frac{dU_e}{dx}\right)_s \frac{D}{U_\infty} = \frac{2}{U_\infty}\sqrt{\frac{2(p_s - p_\infty)}{\rho_s}}$. This formulation, frequently used, neglects the influence of the shock standoff distance on $\frac{dU_e}{dx}$. However, works of [23] and [24] have demonstrated that the tangential velocity gradient depends on the density ratio through the shock and thus the shock standoff distance. Moreover, the influence of the vorticity produced by the shock curvature on the flow is not considered. For high stagnation enthalpy past a curved choc, chemical reactions modify the tangential velocity gradient at stagnation point, which is neglected in this equation. A more complete formulation, taking into account all the phenomena described earlier, has been proposed by Olivier [25]. Olivier's formulation (describing the tangential velocity gradient) associated to the Freeman's equation [26] for the shock standoff distance agrees well with the present CFD results (maximal dispersion of 28%). Prandtl and Lewis numbers can be fixed to classical values used: 0.71 and 1 respectively.

The wall dynamic viscosity μ_w may be computed with the Sutherland's law according to the wall temperature. The wall density ρ_w depends on the compressibility coefficient $Z_w = 1 + Y_A$; where Y_A is the mass fraction of an atom A.

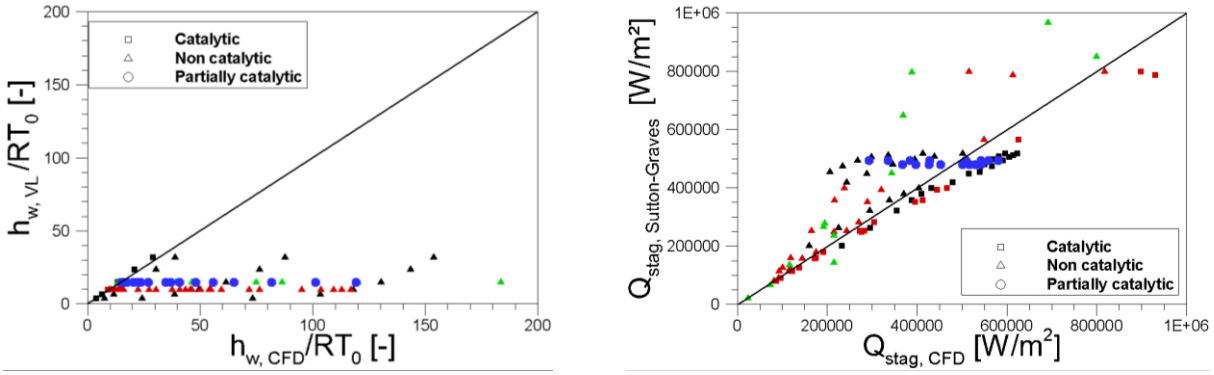

Fig. 5. Comparison between specific enthalpy from CFD and Eq. 6 with $\sum_A Y_A h_A^0 = 0$ (on the left). Comparison between wall heat flux from CFD and Sutton-Graves equations (on the right). Colored symbols represent the effect of the **wall temperature**, curvature radius, flight point and recombination coefficient.

Furthermore, the wall enthalpy is given by Eq. 6, where the specific heat capacity Cp is modeled thanks to Vérant-Lepage equation (Eq. 8) and h_A^0 is the formation enthalpy of a particle A. In Fay-Riddell formulations, $h_w = Cp\,(T_w) \times T_w$ and $h_{De} = \sum_A Y_{Ae} h_A^0$. For a catalytic wall, $\sum_A Y_A h_A^0 = 0$, results from Eq. 6 agree well with CFD as illustrated in Fig. 5 (squares). For non-catalytic or partially catalytic wall, this term must be computed (Eq. 7) to avoid scattered the results (Fig. 5, triangles and circles). For non-catalytic wall, the mass fraction in the boundary layer is constant, $Y_{Ae} = Y_A$, so $h_{De} = \sum_A Y_{Ae} h_A^0 = \sum_A Y_A h_A^0$. Unfortunately, no analytical model is yet available in literature to assess the mass fraction of the atoms at the wall (for non-catalytic wall) or outside the boundary layer (for partially catalytic wall) regardless of the flow conditions.

$$h_w = Cp\,(T_w) \times T_w + \sum_A Y_A h_A^0 \tag{6}$$

$$\sum_A Y_A h_A^0 = Y_O h_O^0 + Y_N h_N^0 + Y_{NO} h_{NO}^0 \tag{7}$$

$$Cp(T_w) = c_1 + c_2 \times \left(\frac{\bar{\theta}_{vib}}{T_w}\right)^2 \frac{e^{\frac{\bar{\theta}_{vib}}{T_w}}}{\left(e^{\frac{\bar{\theta}_{vib}}{T_w}} - 1\right)^2} \tag{8}$$

With $h_O^0 = 1.54 \times 10^7 J/kg$, $h_N^0 = 3.36 \times 10^7 J/kg$, $h_{NO}^0 = 2.99 \times 10^6\ J/kg$, $\bar{\theta}_{vib} = 3000\ K$, $c_1 = 1005\ J\ /\ kg.K$ and $c_2 = 296\ J\ /\ kg.K$.

The stagnation point heat flux computed with the Fay-Riddell and Sutton-Graves equations using the CFD mass fraction of particles has been successfully compared to the CFD stagnation point heat flux, regardless of the wall catalysis (Fig. 6). For the Fay-Riddell equation, minimal, maximal and mean differences with CELHyO stagnation point heat flux is respectively 0%, 15% and 5.6% for a catalytic wall, 0%, 37% and 7% for a non-catalytic wall and 0.25%, 2.3% and 5.2% for a partially catalytic wall.

This demonstrates that, with the correct description of the wall enthalpy, i.e. with wall atomic mass fractions, the equations proposed in literature may be used for catalytic, non-catalytic and partially catalytic walls. Moreover, comparison with the CFD results has confirmed that these equations may be valid for a large range of flight points. The challenge is thus to propose a model for the atomic mass fraction at stagnation point for a finite catalysis of the wall, regardless the flow conditions.

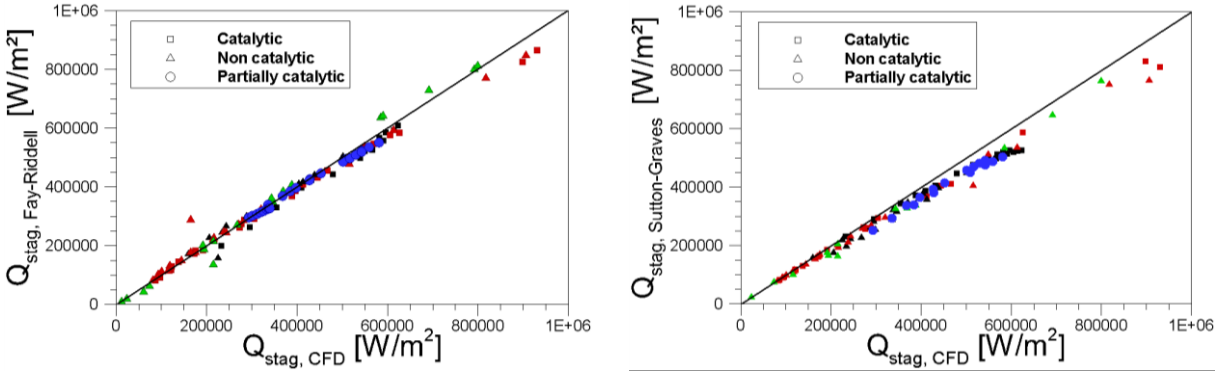

(a) (b)

Fig. 6. Comparison of the CFD stagnation point heat flux with Fay-Riddell (a) and Sutton-Graves (b) heat flux, when these equations use CFD results for the atomic mass fraction.

5 DEVELOPMENT AND VALIDATION OF THE ANALYTICAL MODELS

Following the conclusion of the CFD database analysis and the study of the models proposed in literature, a model for the mass fraction of the atomic species has been proposed for non-catalytic wall.

$$Y_A = f(V_\infty, \rho_\infty, Rn, T_w) \tag{9}$$

Let's assume Y_A as the sum of the mass fractions of the species, i.e. O, N and NO. Since the enthalpy of formation of NO is 10 times inferior to the enthalpy of formation of the atomic species and since the mass fraction of NO in the flow is negligible compared to N and O ones, the term $Y_{NO}h_{NO}^0$ is thus neglected.

Given Y_A, Y_O and Y_N are then deduced as follows:

- If $Y_A < 0.23$, then $Y_O = Y_A$ and $Y_N = 0$
- If $Y_A \geq 0.23$, then $Y_O = 0.23$ and $Y_N = Y_A - Y_O$

For non-catalytic wall, the mass fractions of atomic species thus obtained are used to compute the wall enthalpy thanks to Eq. 6 to 9. Then, the stagnation point heat flux is calculated using the Sutton-Graves or Vérant-Sagnier equations. For the Fay-Riddell formulation, the mass fractions of the atomic species appear in h_{De} and must not be considered twice in h_{De} and h_w. Consequently, the stagnation point heat flux is calculated considering $h_w = Cp\ (T_w) \times T_w$ and $h_{De} = Y_O h_O^0 + Y_N h_N^0$. The wall enthalpy, as well as the stagnation point heat flux computed with Sutton-Graves anf Fay-Riddell are very satisfactory with the Navier-Stokes results issued from a second CFD database (unused for the development of the models) as illustrated by Fig. 7 and Fig. 8. The dispersion of the analytical results has been evaluated by comparison with CFD ones and summarized in Table 1.

For partially catalytic wall, the wall enthalpy has been modelled with a bridging function according to the wall enthalpy for catalytic $h_{w,c}$ and non-catalytic wall $h_{w,nc}$ as well as the recombination coefficient γ:

$$h_{w,pc} = g(h_{w,c}, h_{w,nc}, \gamma) \quad (10)$$

This formulation (Eq. 10) leads to a minimal, maximal and mean discrepancy of 0.5%, 19% and 7.5% respectively in comparison with CFD results (Fig. 9.a). Used in Sutton-Graves equation, the minimal, maximal and mean discrepancy on the stagnation point heat flux are 0.2%, 17% and 9.3% respectively (Fig. 9.b).

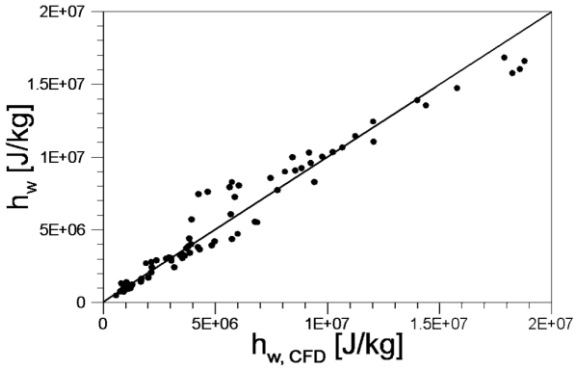

Fig. 7. Comparison between wall enthalpy obtained with CFD and with Eq. 6 coupled to Eq. 9, non-catalytic wall.

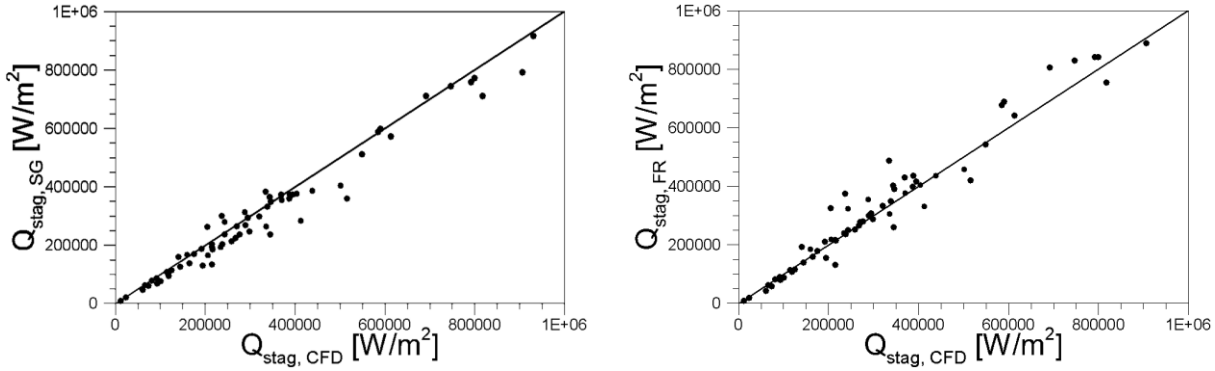

(a) (b)

Fig. 8. Comparison between stagnation point heat flux obtained with CFD and with Sutton-Graves (a) and Fay-Riddell (b) formulations using wall enthalpy computed with the mass fraction model for non-catalytic wall.

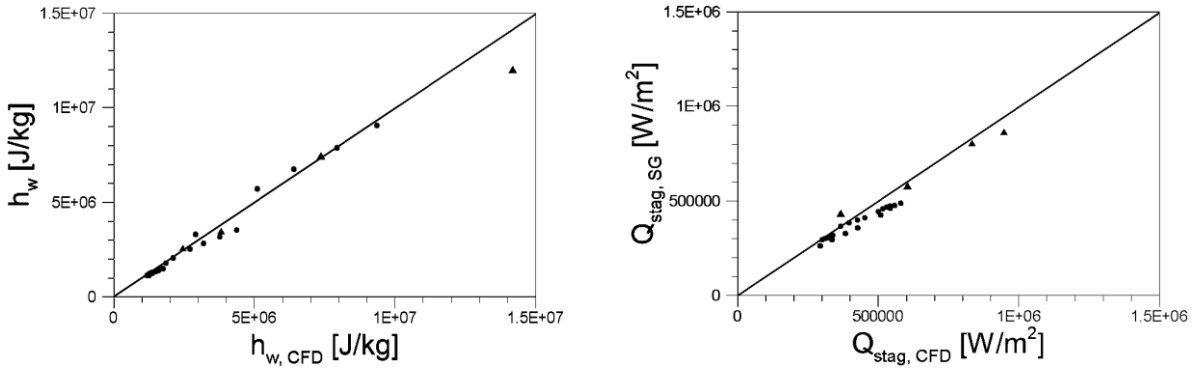

(a) (b)

Fig. 9. Comparison between wall enthalpy and stagnation point heat flux obtained with CFD and with Eq. 10 and Sutton-Graves formulation for finite catalytic wall. Symbols correspond to different test conditions (flight point, nose radius and wall temperature).

These new models for non-catalytic and partially catalytic walls are valid for altitudes between 70 km and 20 km,

flow velocity between 8 km/s and 1 km/s, nose radius between 0.01 m and 10 m and temperature between 300 k and 2000 K.

Table 1. Minimal, maximal and mean discrepancy between stagnation point heat flux computed with analytical models and the numerical results from CFD CELHyO data for catalytic and non-catalytic walls.

	Discrepancy (%)	$Q_{Sutton-Graves}$	$Q_{\text{Vérant-Sagnier}}$	$Q_{\text{Fay-Riddell}}$
Catalytic	Min	8.14	0.48	0.02
	Max	22.73	14.24	14.37
	Mean	13.27	4.85	5.53
Non-catalytic	Min	0.20	0.23	0.12
	Max	36.58	34.10	33.69
	Mean	11.84	12.03	9.20

6 INFLUENCE OF THE WALL CATALYCITY ON THE WALL HEATING ALONG THE ATMOSPHERIC ENTRY

The objective of this re-entry application is to highlight the influence of the wall catalycity on the wall heating which drives the thermal degradation of the space debris during its atmospheric entry. Various ballistic trajectories T1, T2, and T3 have been considered (Fig. 10) from the following initial conditions: $Z = 70\ km$, $V_\infty = 7500\ m/s$ and $-0.1°$ of slope angle. The wall temperature T_w is computed assuming the radiative equilibrium at the wall between the convective heat flux and the radiative cooling. The emissivity and the melting temperature of the material are respectively fixed to 0.75 and 2000 K (corresponding to TA6V usual values).

As illustrated in Fig. 11, regardless of the entry trajectory considered, the wall catalysis of the material has a significant influence on the wall heating and thus on the wall temperature. For the trajectory #3, the thermal degradation of the material increases with the wall catalysis since the melting temperature of the material is reached earlier and is maintained on a more important part of the trajectory for a catalytic wall than for a non-catalytic wall. For the trajectory #2, the melting temperature is not reached for both non-catalytic or finite catalytic wall unlike the catalytic wall case.

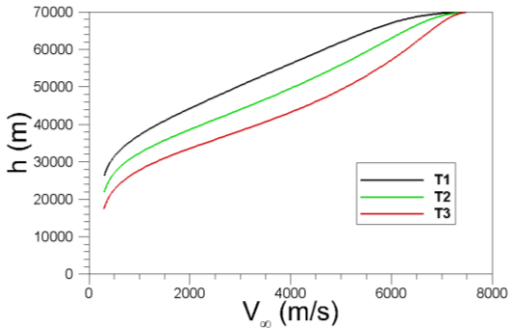

Fig. 10. Atmospheric entry trajectories T1, T2 and T3.

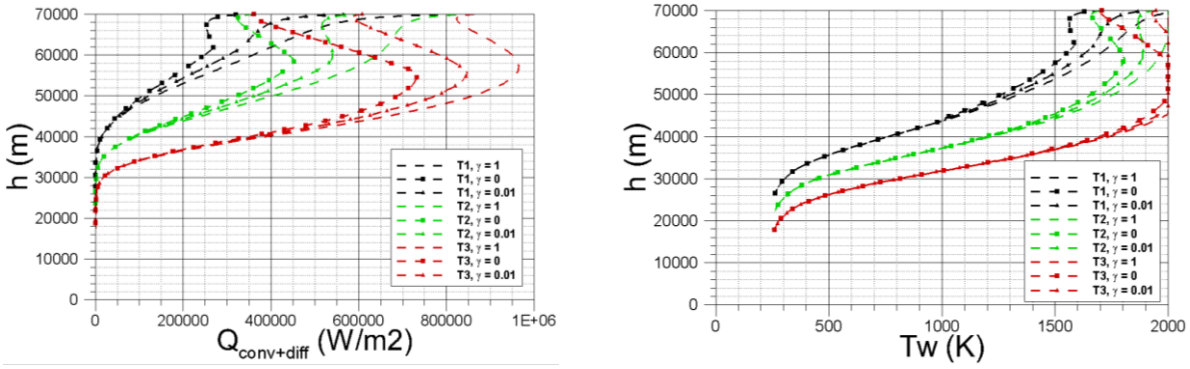

Fig. 11. Influence of the wall catalycity on the stagnation point heat flux and the wall temperature calculated with Sutton-Graves equation for the three trajectories considered.

7 CONCLUSION

Around 200 numerical simulations have been performed with the ONERA Navier-Stokes code CELHyO. This database has been analyzed to identify the driving parameters influencing the wall stagnation point heat flux for non-catalytic and partially catalytic walls. Usual analytical models from open literature and mainly used in engineering codes have been reviewed to highlight their shortcomings in the proper description of wall heating in a parametrical study of re-entry debris flights. A model for mass fraction of the atomic species at wall has been developed for non-catalytic walls. The proposed model aims at properly representing the wall enthalpy used in the stagnation point heat flux equations proposed in literature. For partially catalytic walls, a specific bridging function has been developed for assessing the wall enthalpy. The accuracy of these models has been estimated according to variation of flight point conditions, nose radii and wall temperatures. The results exhibit significant improvements compared to available models in engineering codes to simulate stagnation point heat flux for non-catalytic and partially catalytic walls. Finally, the significant influence of the wall catalycity on the calculation of the wall temperature and thus on the thermal wall degradation has been demonstrated along complete atmospheric entry trajectories.

8 REFERENCES

1. Orbital debris quarterly news, May 2019. https://orbitaldebris.jsc.nasa.gov/quarterly-news/pdfs/odqnv23i1.pdf
2. ESA. Space operation, Space debris: the ESA approach. ESA Space Debris brochure 2017.
3. W.Ailor, W. Hallman, G. Steckel, M. Weaver. Analysis of reentered debris and implications for survivability modelling. In: 4th European Conference on Space Debris, 2005.
4. N.L.Johnson. Space debris modeling at NASA. In: 3rd European Conference on Space Debris, 2001.
5. E.V.Zoby, K.P.Lee, R.N.Gupta, R.Thompson. Nonequilibrium Viscous Shock Layers Solutions for Hypersonic Flow Over Slender Bodies. Paper No. 71, Eighth National AeroSpace Plane Technology Symposium, 1990.
6. C.Martin, C.Brandmueller, K.Bunte, J.Cheese, B.Fritsche, H.Klinkrad, T. Lips, N. Sanchez. A debris risk assessment tool supporting mitigation guidelines. In: 4th European Conference on Space Debris, 2005.
7. P.Omaly, C.Magnin-Vella, S.Galera. DEBRISK, CNES tool for re-entry survivability prediction: validation and sensitivity analysis. In: 6th IAASS Conference, 2013.
8. C.D.Scott, R.C.Ried, R.J.Maraia, C.P.Li, S.M.Derry. An AOTV Aeroheating and Thermal Protection Study. Nelson ed., Thermal Design of Aeroassisyed Orbital Transfer Vehicles, *prog. Astronautics Aeronautics*, 1985.
9. P.Sagnier,J-L.Vérant. Flow Characterization in the ONERA F4 high enthalpy wind tunnel, *AIAAJ*. 36 (4), 1998.
10. R.W.Detra, N.H.Kemp, F.R.Riddell. Addendum to Heat transfer to Satellite Vehicle Reentering the Atmosphere. Jet Propulsion, Vol. 27, No. 12, 1957.
11. T.Lips, B.Fritsche, M.Homeister, G.Koppenwallner, H.Klinkrad, M.Toussaint. Re-entry Risk Assessment for Launchers – Development of the New SCARAB 3.1L. In: 2nd IAASS Conference, 2007.
12. J.Annaloro, P.Omaly, V.Rivola, M.Spel. Elaboration of a New Spacecraft-Oriented Tool: PAMPERO. In: 8th European Symposium on Aerothermodynamics for Space Vehicles, 2014.
13. Y.Prévereaud, J.-L.Vérant, M.Balat-Pichelin, J.-M.Moschetta. Numerical and experimental study of the thermal degradation process during the atmospheric re-entry of a TiAl6V4 tank. *Acta Astonautica*, 122: 258-286, 2016.
14. T.Lips. Equivalent Re-entry Breakup Altitude and Fragment List. In: 6th European Conf. on Space Debris, 2013.
15. S.Reggiani, C.Bruno, M.Barbato, J.Muylaert. Model for heterogeneous catalysis on metal surfaces with applications to hypersonic flow. AIAA Meeting Paper. In: AIAA Thermophysics Conference, 1996.
16. J.J.Bertin. Hypersonic Aerothermodynamics. AIAA Education Series, 1938.
17. R.Goulard. On Catalytic Recombination Rates in Hypersonic Stagnation Heat Transfer. *Jet Propulsion*, 1958.
18. B.Halpern, D.E. Rosner. Chemical Energy Accommodation at Catalyst Surfaces. *Chemical Society of London Faraday Transaction I Physical Chemistry*, Vol. 74, Part 8, pp. 1883-1978, 1978.
19. G.A.Mellin, R.J.Maddix. Energy Accommodation during Oxygen Atom Recombination on Metal Surfaces. *Faraday Society Transactions*, Vol. 67, 1971.
20. C.D.Scott. Catalytic Recombination of Nitrogen and Oxygen on High-Temperature Reusable Surface Insulation. *AIAA Paper*, 1980.
21. J.A.Fay, F.R.Riddell. Theory of Stagnation Point Heat Transfer in Dissociated Air. *Journal of the Aeronautical Sciences*, Vol. 25, No. 2, pp.73-85, 1958.
22. L.Lees. Hypersonic flow. Proc. 5th Int. Aero. Conf. IAS-RAeS, Los Angeles, 241-276, 1956.
23. W.D.Hayes, R.F.Probstein. Hypersonic flow theory, inviscid flow. Academic Press, New York, London, 1966.
24. T.Y.Li, R.E. Geiger. Stagnation point of a blunt body in hypersonic flow. *J. Aer Sci* 24:25-32, 1957.
25. H.Olivier. Influence of the velocity gradient on stagnation point heating in hypersonic flow. Shock Waves, 1995.
26. N.C.Freeman. On the theory of hypersonic flow past plane and axially symmetric bluff bodies. *J. Fluid Mech*, 1956.
27. K.Sutton, R.A.Graves Jr. A General Stagnation-Point Convective Heating Equation for Arbitrary Gas Mixtures. NASA TR R-376, 1971.